CrystEngComm

ROYAL SOCIETY OF CHEMISTRY

PAPER

View Article Online
View Journal | View Issue

Cite this: *CrystEngComm*, 2020, **22**, 3463

Solution and calorimetric thermodynamic study of a new 1 : 1 sulfamethazine–3-methylsalicylic acid co-crystal†

Dipali Ahuja, [a] Michael Svärd, *[b] Matteo Lusi [a] and Åke C. Rasmuson[ab]

A new 1 : 1 co-crystal of sulfamethazine (API, SMT) and 3-methylsalicylic acid (coformer, 3mSA) has been synthesized and its crystal structure solved by single crystal X-ray diffraction (XRD). The co-crystal has been thoroughly characterized by powder XRD, thermogravimetric analysis (TGA) and differential scanning calorimetry (DSC). The pure co-crystal could be synthesized by solvent drop grinding, cooling crystallization and slurry conversion co-crystallization. Ternary phase diagrams have been constructed in methanol and acetonitrile at 30 °C. The co-crystal exhibits incongruent dissolution in both solvents. The thermodynamics of co-crystal formation have been estimated from solubility data and calorimetric data, respectively, showing that formation of the SMT–3mSA co-crystal from its solid components is spontaneous and entropy-driven. The co-crystal formation is associated with a 5% increase in molecular volume. A relationship between the size of the region where the co-crystal is the most stable solid phase and the relative solubility of the co-crystal components has been uncovered. The co-crystal region becomes smaller as the solubility ratio increases.

Received 2nd April 2020,
Accepted 3rd May 2020

DOI: 10.1039/d0ce00498g

rsc.li/crystengcomm

Introduction

Many active pharmaceutical ingredients (APIs) fall in the Biopharmaceutics Classification System (BCS) class II category, signifying a high permeability but low solubility.[1] Hence, development of new opportunities and techniques to improve and control the pharmacological properties of APIs is vital.[2] Both crystalline and amorphous solid forms can be exploited, but the former is preferable for meeting specifications related to stability, purity and processing.[3] Modification of crystal packing and intermolecular interactions of molecules directly affects the physicochemical properties. This approach is called crystal engineering[3] and has facilitated tailoring of solid forms with enhanced desirable properties such as solubility,[4] hygroscopicity,[5] stability,[6,7] and bioavailability.[8]

Co-crystals are single-phase crystalline solids composed of two or more different components in a specific stoichiometric ratio.[9] Molecules of any shape or size possessing complementary bonding functionalities can lead to co-crystal formation. They are held together by non-covalent interactions, the most important being hydrogen bonding because of its directional nature. The "pK_a rule" is often used to predict whether an acid–base pair of compounds will crystallise as a salt or a co-crystal. The rule states that salt formation generally requires a difference of about 3.0 pK_a units between the conjugate acid form of the base (protonated form) and the acid, *i.e.* ΔpK_a = [pK_a (base) − pK_a (acid) ≥ 3.0]. If the pK_a of acid is greater than that of the protonated base leading to a negative ΔpK_a value, this most likely leads to the formation of a co-crystal. The prediction is not very accurate for ΔpK_a values between 0 and 3, for which either a salt or a co-crystal could form.[10,11]

A number of co-crystals have been reported in the literature for different APIs, and the number is continuously increasing. For the API in this study, sulfamethazine (SMT), which exists as a single polymorphic form, the number of co-crystals reported in the literature is around 33.[12] A few solvates for SMT are also reported in the literature.[13] SMT is an antimicrobial and anti-infective agent, used as a veterinary medicine and for treatment of malaria, rheumatoid fever and toxoplasmosis in humans. The coformer, 3-methylsalicylic acid (3mSA), also known as 2,3-cresotinic acid, *o*-cresotinic acid and hydroxytoluic acid, is a derivative of salicylic acid. There are no polymorphs known for 3mSA in the open literature. It has a marked fibrinolytic activity in human plasma. The chemical structures of the API, SMT and the coformer, 3mSA are shown in Fig. 1.

[a] *SSPC, the SFI Research Centre for Pharmaceuticals, Bernal Institute, Department of Chemical Sciences, University of Limerick, Co. Limerick, Ireland*
[b] *Department of Chemical Engineering, KTH Royal Institute of Technology, Teknikringen 42, SE-10044 Stockholm, Sweden. E-mail: micsva@kth.se*

† CCDC 1991374. For crystallographic data in CIF or other electronic format see DOI: 10.1039/d0ce00498g

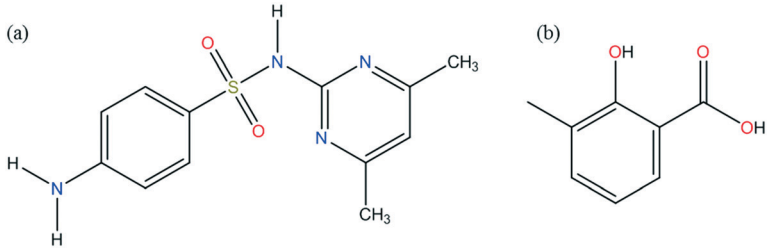

Fig. 1 Chemical structures of sulfamethazine (a) and 3-methylsalicylic acid (b).

For robust industrial manufacturing of co-crystals, the size, shape and location of the co-crystal region in the phase diagram is of importance. The appearance and symmetry of the phase diagram depends on the components as well as the solvent. A co-crystal can show congruent or incongruent dissolution, leading to symmetric or asymmetric phase diagrams. However, the factors that cause and control the co-crystal dissolution behaviour are not clear. In previous work, we have shown that the solubility ratio between the pure co-crystal components cannot be used to reliably predict the co-crystal dissolution behaviour.[14] However, it has also been shown that pure co-crystal can still be isolated regardless of whether the system is congruent or incongruent.[14]

In the literature, a few co-crystals have resulted in an improved bioavailability of the poorly soluble API.[15–17] The co-crystal solubility is an important parameter, indicative of bioavailability, but for incongruent systems measurement of solubility by traditional methods is not possible. Co-crystal solubility can be represented in terms of the solubility product, which includes the concentration of both solid components.[18] The true indicator of co-crystal stability is the Gibbs energy, but there are few studies in the literature dedicated to the thermodynamics of co-crystal formation.[19]

In this work, a new 1 : 1 co-crystal between SMT and 3mSA has been manufactured, and the crystal structure solved and characterized using X-ray diffraction (XRD), thermogravimetric analysis (TGA) and differential scanning calorimetry (DSC). The ternary phase diagrams of this 1 : 1 co-crystal system have been constructed in two solvents, methanol and acetonitrile, at 30 °C. The thermodynamic functions of co-crystal formation have been estimated using solubility and calorimetric data. A relationship between the size of the region in the ternary phase diagram where the co-crystal is the stable solid phase and the coformer to API solubility ratio is shown in the present work.

Experimental work

Materials

Sulfamethazine (CAS Registry Number 57-68-1), purity >99%, 3-methylsalicylic acid (CAS Registry Number 83-40-9), purity >97% and methanol (CAS Registry Number 67-56-1, HPLC grade, purity >99.9%) were purchased from Sigma-Aldrich. Acetonitrile (CAS Registry Number 75-05-8, HPLC grade, purity >99.9%) was purchased from Fisher Chemicals. All the chemicals were used as received.

Solid state analysis

Single-crystal X-ray diffraction measurements for structural determination of the 1 : 1 SMT–3mSA co-crystal were collected at 104 K using a Bruker Quest D8 diffractometer with Mo K_α (λ = 0.7093 Å) radiation. The diffractometer was equipped with CMOS photon detector. Data were corrected for absorption using empirical methods (SADABS) based upon symmetry-equivalent reflections combined with measurements at different azimuthal angles. The structure was solved with the SHELX structure solution program using direct methods and refined with the Olex2 refinement package using Gauss–Newton minimisation. Non-hydrogen atoms were refined anisotropically and hydrogen atoms were placed in calculated positions refined using idealized geometries (riding model) and assigned fixed isotropic displacement parameters.

Powder X-ray diffraction (PXRD) data were collected in reflectance mode using an Empyrean diffractometer (PANalytical, Philips) equipped with Cu $K_{\alpha1,2}$ radiation (γ = 1.5406 Å) operating at 40 kV and 40 mA at room temperature. Samples were scanned between 2θ values of 5 and 40° at a step size of 0.01313° 2θ with step time 73 s per step on a spinning silicon holder.

An Agilent Technologies 1260 Infinity Series setup comprising a 1260 Quat solvent delivery pump, auto injector, absorbance UV spectrophotometric detector (275 nm) and Agilent ChemStation software was used for HPLC analysis. A Macherey-Nagel EC 100/4.6 Nucleodur C18 column was used. Methanol and 2% (v/v) acetic acid in water in the volume ratio 88 : 12 were used as the mobile phase.

A TA Instruments Q50 V20.13 Build 39 under nitrogen environment was used to perform thermogravimetric analysis (TGA) experiments. Samples were placed on open platinum pans and heated up to 773 K at a ramp rate of 20 K min^{-1}.

Melting temperatures and associated enthalpies of fusion were determined using a TA Instruments Q2000 differential scanning calorimeter, at a constant heating rate of 3 K min^{-1}. In all DSC experiments, evenly distributed powder samples of approx. 5 mg were encapsulated in Tzero aluminum pans, the furnace was purged with nitrogen gas at 50 mL min^{-1}, and the instrument was calibrated against the melting

properties of indium. The heat capacity signal was calibrated using a linear function of temperature against a sapphire sample. Sample weights were re-measured after each run to verify that no mass loss due to sublimation, evaporation or degradation had occurred.

Preparation of co-crystal

The co-crystal was initially synthesized using the solvent drop grinding method. Equimolar amounts of sulfamethazine (SMT) and 3-methylsalicylic acid (3mSA) were weighed. The mix was finely ground with a few drops of acetonitrile for about 15–20 minutes by hand using a pestle and mortar. The resulting white powder was characterized by PXRD and DSC. Slurry conversion co-crystallization (explained below) was employed for the co-crystal synthesis for ternary phase diagram investigations.

Measurement of solubility

Solubility of SMT and 3mSA in acetonitrile and methanol at 30 °C was determined by a gravimetric technique explained previously.[14] An OHAUS Explorer analytical balance with a resolution of 10^{-4} g was used for weighing of chemicals. The experiments were carried out in 30 mL glass vials with magnetic stirrer bars. The water bath setup comprised a Grant ST26 stainless steel thermostatic water bath; 26 L, 505 × 300 × 200 mm; equipped with a Grant C2G cooling unit and a Grant GR150 control unit; stability ±0.01 °C and uniformity ±0.05 °C with a serial submersible 60 points magnetic stirrer plate (2Mag) placed on the base and a submersible water pump (1400 L h^{-1}) to enhance circulation in the bath. For each solute, an amount of solid material in excess of solubility was added to 5 mL solvent at 30 °C and allowed to reach equilibrium under stirring. After 24 hours, the agitation was stopped and the solids allowed to settle for a period of 15–20 minutes. 1 mL of the clear, saturated liquid above the solid was pipetted out using a pre-heated syringe and filtered through a 0.2 μm PTFE syringe filter into a pre-weighed pre-heated glass vial (m_1). The vial was then weighed immediately and the mass recorded as m_2. The solvent was then allowed to evaporate by placing the vial for a sufficient time (usually overnight) in the fume hood until visually dry and the mass recorded. The mass at the point where no further decrease could be observed was considered to be the mass of the dry vial (m_3). The solubility was then calculated using $(m_3 - m_1)/(m_2 - m_3)$ as g of solute per g of solvent. In each case, three repeats were performed. To confirm the identity of the solid form, the solid material in the equilibrium slurry was sampled and analysed by PXRD.

Construction of the ternary phase diagram and determination of invariant points

Phase diagrams for this co-crystal system were constructed in two solvents (methanol and acetonitrile) at 30 °C. Slurry conversion was employed to determine the invariant points by equilibrating several mixtures of the two solid co-crystal components with the solvent. The solid and the solution phases were then analysed. At 30 °C, SMT and 3mSA were mixed with the solvent and stirred for 72 hours, a time sufficient to reach equilibrium. Preliminary experiments were performed to establish the equilibration time. Slurry experiments were run for different times, starting from 24 hours and gradually increasing the time until constant concentrations of SMT and 3mSA were reached at 48 hours. The suspension was left to stand to allow sedimentation of the solid material. The saturated solution was withdrawn and filtered into two aliquots. The solid material was analyzed by PXRD. One aliquot of the liquid was diluted by pure solvent and examined by HPLC. The concentration of SMT and 3mSA was determined from calibration curves in the pure solvent. The second aliquot of the liquid phase was evaporated to dryness to determine the total dissolved solute in the liquid phase by gravimetry. The solubility of the pure components and the composition of the invariant points were converted to mass fraction on a total mass basis and plotted using the Prosim Ternary Diagram software.[20]

Single crystal preparation

The ternary phase diagram was used as guidance to identify a composition where the 1:1 co-crystal was the most stable solid phase. SMT, 3mSA and acetonitrile were mixed in the corresponding ratio and the mixture was allowed to stir at 30 °C. The saturated solution was withdrawn with a pre-heated syringe, filtered into a preheated glass vials, and heated to 30 °C for 30 minutes. The solution was then allowed to stand at 20 °C in a temperature-controlled water bath until single crystals were obtained. The crystals were isolated, surface dried on Whatman filter paper before PXRD analysis was carried out.

Results and discussion

Solid phase and crystal structure analysis

The crystallographic data obtained for the 1:1 co-crystal between SMT and 3mSA is summarized in Table 1.

The crystal structure belongs to the *Pbca* space group (orthorhombic). Fig. 2 depicts the molecular packing and hydrogen bond pattern present in the co-crystal. The asymmetric unit of the SMT–3mSA co-crystal comprising one molecule of SMT and one molecule of 3mSA is held by a $R_2^2(8)$ hydrogen bond motif between the 3mSA carboxylic acid and the amide tautomer of SMT. The N–H—O bond between SMT sulfonamide and 3mSA carbonyl, and the O–H—N bond between 3mSA hydroxyl and SMT pyrimidine nitrogen, are key components of the crystal structure. The phenyl ring of 3mSA shows π–π interactions with both the pyrimidine (parallel displacement) and phenyl ring (T-shaped) of SMT. Two SMT molecules are held together by hydrogen bonds of the type N–H—O. Each SMT molecule is bonded to two other SMT molecules and one 3mSA molecule. The dihedral angle between the two rings (phenyl and pyrimidine) in SMT of the co-crystal, 72.11° is close to the corresponding angle, 75.55°

Table 1 Crystallographic data for the 1:1 SMT–3mSA co-crystal

	SMT–3mSA co-crystal
Stoichiometry	1:1
Empirical formula	$C_{20}H_{22}N_4O_5S$
Formula mass	430.48
Temperature (K)	104
Crystal system	Orthorhombic
Space group	*Pbca*
a (Å)	11.0926 (6)
b (Å)	14.8423 (8)
c (Å)	25.6676 (14)
α (°)	90
β (°)	90
γ (°)	90
V (Å^3)	4225.9 (4)
Z	8
P_{calc} (g cm^{-3})	1.353
R-factor (%)	5.35
μ (mm^{-1})	0.192
θ (max)	28.456
N_{ref}	5330
N_{par}	274
Goodness-of-fit (GOF)	1.159

in pure SMT, which is a monomorphic system.[21] The angles around the trigonal carbon in 3mSA of the co-crystal, 115.83° and 121.60°, are similar to those observed in pure 3mSA.[22] The central 'S' atom in the SMT molecule, both in single and multicomponent crystal structures, shows tetrahedral geometry. The angle in pure SMT is ~108.2°, and that in the co-crystal is ~107.8°.

The optical micrograph of the co-crystal single crystal shows a plate-like crystal habit as seen in Fig. 3.

The experimental PXRD pattern recorded for the co-crystal matches well with the that calculated (using the software Mercury) from the crystal structure determined by the single crystal-XRD (Fig. 4a). In addition, the co-crystal pattern is unique as compared to the pure components, indicating the formation of a new solid phase (Fig. 4b).

The crystal structure determination suggests that the solid is a co-crystal as opposed to a salt. The two C–O bond lengths for the carboxylate group of the coformer, 3mSA are 1.242 and 1.302 Å, bringing the difference to 0.06 Å. This is similar

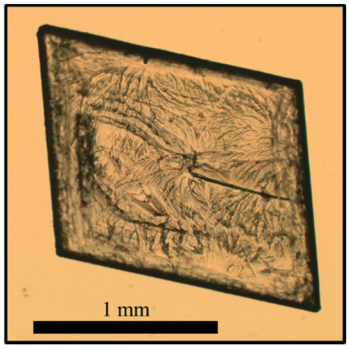

Fig. 3 Micrograph obtained by optical microscopy of a single SMT–3mSA co-crystal.

to the case of the SMT–salicylic acid co-crystal, where the difference between the two C–O bond lengths is 0.049 Å (GEYSAE).[23] For salts, this difference is usually less than 0.03 Å as the carboxylate ion, formed after proton loss goes into resonance.[24] Using 2.65[25] as pK_1 value for the conjugate acid form of the basic SMT and 2.95[26] as pK_1 value for 3mSA, ΔpK_a becomes −0.3, which according to the pK_a rule also suggests that SMT–3mSA should form a co-crystal as opposed to a salt.[27] These pK_a values correspond to the amino functional group of the basic API and to the carboxylic group of the acidic coformer. The interactions in the co-crystal occur through the sulfonamide group of the API and the carboxylic group of the coformer. It is interesting to note that the amino group, based on which the pK_a rule is applied does not interact with the coformer. The geometric and steric factors ensure that the system assembles in a way to minimize the free energy. This indicates that, although the pK_a rule can act as a guide in predicting whether a salt or co-crystal will form, it is not completely reliable.

Thermal analysis and solid phase thermodynamics

TGA curves for the three pure solid phases SMT, 3mSA and co-crystal are presented in Fig. 5. There is no indication of any bound solvent in either of the solids. For 3mSA, the mass

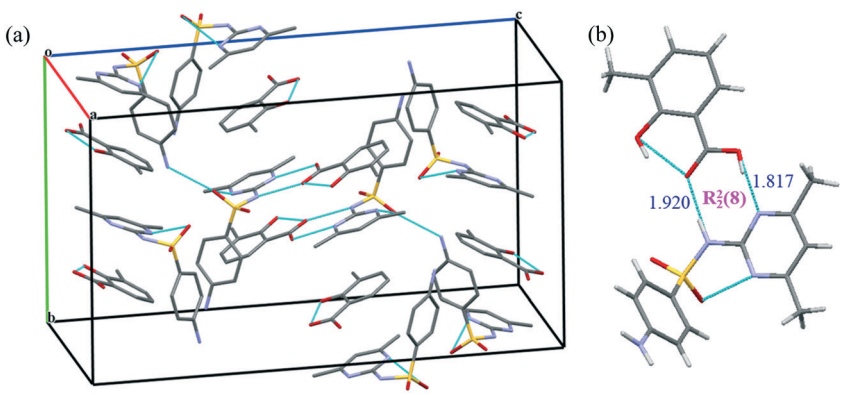

Fig. 2 Unit cell of the 1:1 SMT–3mSA co-crystal depicting the crystal packing and bonding pattern (a), hydrogen bonding forming a $R_2^2(8)$ moiety in the SMT–3mSA co-crystal, distances in Å (b).

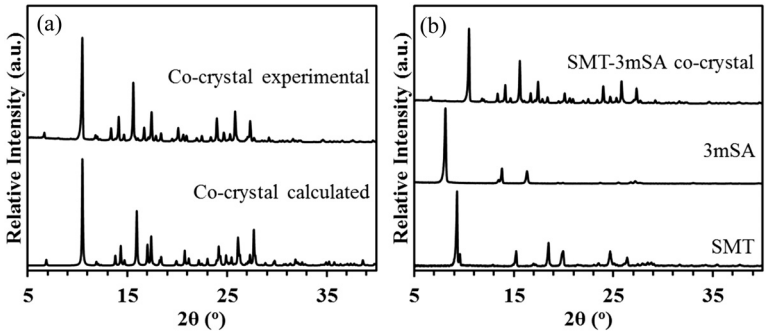

Fig. 4 Experimental and simulated PXRD patterns for the 1:1 SMT–3mSA co-crystal (a); comparison of PXRD patterns between the SMT–3mSA co-crystal with SMT and 3mSA (b).

starts to decrease at around 420 K, and at 500 K virtually all the 3mSA has been lost, due to sublimation, evaporation and/or degradation. The co-crystal curve exhibits a similar tendency, with an onset of mass loss at approximately 440 K. At 520 K, there is a slight change in the slope of the co-crystal TGA curve, and by then 35% of the initial mass has been lost, corresponding to the loss of a stoichiometric amount of 3mSA from the 1:1 co-crystal; the molar masses of SMT and 3mSA being 278.33 g mol^{-1} and 152.15 g mol^{-1}, respectively. This temperature value corresponds well to the point where the TGA curve for pure SMT begins to decrease. Both the SMT and the co-crystal curves then proceed to decay further in a similar fashion.

The DSC traces for the pure co-crystal and for the two respective pure components each show a single endothermic melting peak; Fig. 6. The extrapolated onset melting temperatures and the associated enthalpies of fusion of the co-crystal and 3mSA were determined as averages of either 4 or 5 repeat DSC runs. The data is given in Table 2 together with data for SMT from previous work.[28] The melting point of the co-crystal (453.0 K) is intermediate between that of pure SMT (469.7 K) and pure 3mSA (436.5 K). Notably, the molar values of the enthalpy and entropy of fusion for the co-crystal are significantly higher than for the pure components, but the sum of the values of the pure components exceeds the value for the co-crystal, both with respect to enthalpy (5.1 kJ mol^{-1}) and entropy (10.5 J mol^{-1} K^{-1}) (please note that one mole of co-crystal consists of one mole each of API and coformer). This suggests that the co-crystal has a higher, less favourable enthalpy than the sum of its components, but also a higher, more favourable entropy. However, since these phase transitions occur at different temperatures, an exact comparison cannot be done without making temperature corrections using heat capacity data.

The DSC thermogram for the equimolar physical mixture of API and coformer (Fig. 6) exhibits two discrete endothermic peaks. The first is a faint endothermic event (shown in inset) with an onset at 406 K (standard error = 1.3 K) and an enthalpy of 6.6 kJ mol^{-1} (standard error = 0.11 kJ mol^{-1}), as averaged over four repeat scans. This is followed by a melting peak that matches the melting peak of the co-crystal with respect to both onset temperature and enthalpy to within the levels of experimental uncertainty. From this, it

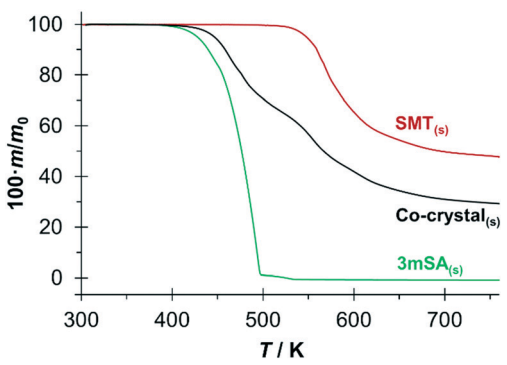

Fig. 5 TGA curves of the 1:1 SMT–3mSA co-crystal and its pure components.

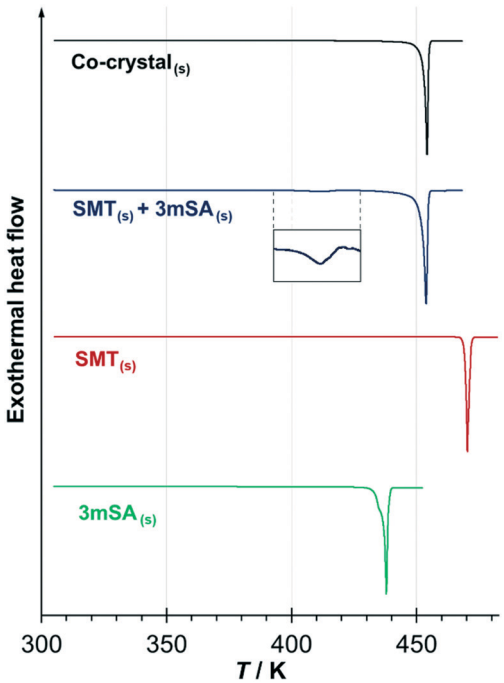

Fig. 6 DSC thermograms of the 1:1 SMT–3mSA co-crystal, the pure components (SMT and 3mSA) and an equimolar physical mixture of the solid components.

Table 2 Melting point data for the three pure solids SMT, 3mSA and the co-crystal, together with standard errors over N repeat experiments

	Sulfamethazine[28]	3-Methylsalicylic acid	1 : 1 co-crystal[a]
T_m/K [N]	469.66 ± 0.03 [4]	436.5 ± 0.21 [4]	453.04 ± 0.09 [5]
$\Delta^{fus}H$ (T_m)/kJ mol^{-1}	36.0 ± 0.14	25.71 ± 0.09	56.6 ± 0.19
$\Delta^{fus}H$ (T_m)/kJ g^{-1}	0.129 ± 0.0005	0.169 ± 0.0006	0.132 ± 0.0004
$\Delta^{fus}S$ (T_m)/J K^{-1} mol^{-1}	76.7 ± 0.30	58.9 ± 0.22	125.0 ± 0.42
$\Delta^{fus}S$ (T_m)/J K^{-1} g^{-1}	0.275 ± 0.0011	0.387 ± 0.0015	0.290 ± 0.0010

[a] 1 mole co-crystal = 1 mol API + 1 mol coformer.

may be concluded that the endotherm at 406 K corresponds to the spontaneous, solid–solid transformation of the equimolar mechanical mixture into the co-crystal.

The Gibbs energy of formation of a solid co-crystal (AB), $\Delta^{form}_{AB}G$ at temperature T in relation to the solid components (A and B) in the solid state can be written as:

$$\Delta^{form}_{AB}G = \Delta^{form}_{AB}H - T\Delta^{form}_{AB}S = G^{s}_{AB} - G^{s}_{A} - G^{s}_{B} \quad (1)$$

A negative Gibbs energy of co-crystal formation signifies that the molecular-level process of mixing equal parts of the two solid components and forming the co-crystal structure is spontaneous. $\Delta^{form}_{AB}G$ consists of an enthalpic and an entropic component. Generally, the enthalpy term is expected to be negative, indicating increased bonding in the co-crystal, and favouring co-crystal formation, while the entropy term often appears to be negative, working against co-crystal formation.[29–32]

Occasionally,[33] notably including the 1 : 1 co-crystal between SMT and salicylic acid (SA),[14] the reverse relationship is observed, meaning the process of co-crystal formation is endothermic, and an increase in entropy drives the process. As can be directly observed, *cf.* the thermograms in Fig. 6, formation of the 1 : 1 SMT–3mSA co-crystal from an equimolar mixture of API and coformer is endothermic at elevated temperatures (6.6 kJ mol^{-1} at 406 K). However, the co-crystal formation still occurs spontaneously at 406 K. This shows that the Gibbs energy of co-crystal formation is negative, and that the process accordingly has to be driven by a favourable entropy increase, similarly as for the 1 : 1 SMT–SA co-crystal.[14]

The entropy increase occasionally observed in co-crystal formation has been proposed to be associated with a volume increase.[29,34] If one molecule of co-crystal (AB) is defined as one molecule of each component (A and B), the increase in molecular volume can be calculated as:

$$\Delta V^{form}_{AB} = \frac{V^{cell}_{AB}}{Z_{AB}} - \left(\frac{V^{cell}_{A}}{Z_{A}} + \frac{V^{cell}_{B}}{Z_{B}}\right) \quad (2)$$

where Z_i denotes the number of molecules in the unit cell of i. Using data from the Cambridge structural database for the structures SLFNMD10 (SMT),[35] CRESOT10 (3mSA)[22] and comparing with the structural data for the co-crystal, Table 1, the increase in molecular volume on co-crystal formation was estimated to 26.3 Å^3 per co-crystal molecule compared to one molecule each of the API and the coformer, or 5%. Notably, the data for the structures of the solid API and coformer is valid at room temperature (283–303 K), while the data for the co-crystal was collected at 104 K. Given a positive thermal expansion coefficient, both the unit cell volume of the co-crystal at 293 K and the true expansion on co-crystal formation at this temperature would be even larger. It has been suggested that an increased degree of hydrogen bonding often serves to counteract close packing and accordingly results in a volume increase.[36] A comparison of the three respective crystal structures shows that the SMT molecule is able to participate in additional hydrogen bonding interactions within the co-crystal lattice compared to in the pure component crystal structure.

Solubility and phase diagrams

The solubility data for SMT and 3mSA in acetonitrile and methanol at 30 °C are listed in Table 3. In both solvents, the order of solubility is same, the coformer 3mSA being is significantly more soluble than the API, SMT. The solubility ratio of 3mSA to SMT in methanol (41.7) is notably higher than in acetonitrile (6.2).

The ternary phase diagrams for the 1 : 1 SMT–3mSA co-crystal in acetonitrile and methanol are depicted in Fig. 7 and 8, respectively. The choice of mass fraction over mole fraction was made to enhance the visibility of the solubility curves in the ternary phase diagrams. The 1 : 1 stoichiometric line does not intersect the co-crystal solubility curve and accordingly the co-crystal shows incongruent dissolution in both solvents. Additional slurry experiments confirmed the nature of incongruent dissolution for the SMT–3mSA co-crystal. In both solvents, excess of pure co-crystal, transformed to a mixture of SMT and co-crystal. In methanol, with a higher solubility ratio of coformer to API, the co-crystal region in the ternary phase diagram is skewed more towards the more soluble component 3mSA side, and is very

Table 3 Solubility of sulfamethazine (SMT) and 3-methylsalicylic acid (3mSA) in methanol and acetonitrile at 30 °C

Solvent	Solubility (mol L^{-1}) SMT	3mSA	Solubility ratio (3mSA/SMT)	Dissolution behaviour
Acetonitrile	0.0592	0.3675	6.2	Incongruent
Methanol	0.0650	2.7121	41.7	Incongruent

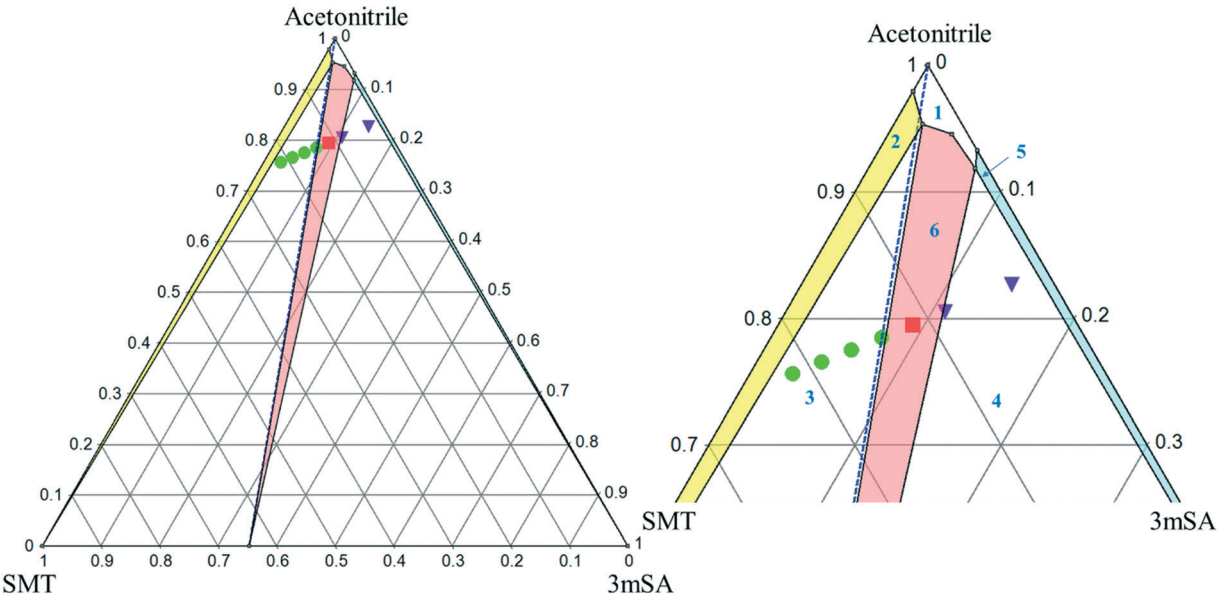

Fig. 7 Full scale (left) and zoom-in view of ternary phase diagram of SMT–3mSA co-crystal system in acetonitrile at 30 °C. Values are in mass fractions. The blue dotted line is the 1 : 1 molar stoichiometric line. Regions in the diagram are as follows: (1) solution phase; all other regions consist of a saturated solution in contact with (2) SMT, (3) SMT + co-crystal (green filled circles), (4) 3mSA + co-crystal (purple inverted triangles), (5) 3mSA, (6) co-crystal (red filled squares). The points-inverted triangle, filled circle and filled square represent experimental data.

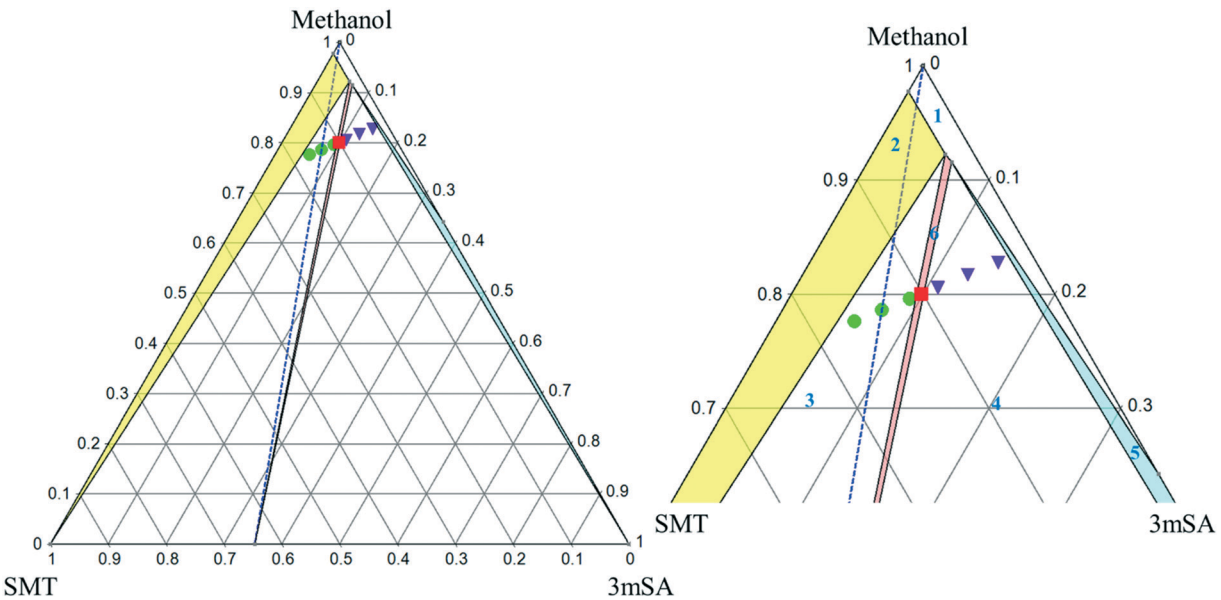

Fig. 8 Full scale (left) and zoom-in view of ternary phase diagram of SMT–3mSA co-crystal system in methanol at 30 °C. Values are in mass fractions. The blue dotted line is the 1 : 1 molar stoichiometric line. Regions and various points are same as marked in Fig. 7.

narrow. In acetonitrile, the co-crystal region is broader, although still skewed towards the coformer side.

The invariant points are the solution concentrations at which two solid phases are stable and simultaneously in equilibrium with the solution. The compositions in mole fractions are given in Table 4. The phase diagrams in Fig. 9 show the incongruent nature in the two solvents and highlight the contrast in the sizes of regions where the co-crystal is stable. Dissolution of the pure 1 : 1 co-crystal in either solvent is thermodynamically expected to lead to the formation of solid SMT or a mixture of SMT and co-crystal depending on the quantity of solvent and extent of dissolution. Likewise, evaporation of a solution at 30 °C containing a stoichiometric 1 : 1 mixture of SMT and 3mSA in methanol or acetonitrile would not (from a thermodynamic point of view) lead to the formation of pure co-crystal. This can be analysed by following the 1 : 1 stoichiometric line joining the solvent vertex and the 1 : 1 co-crystal composition

Table 4 Equilibrium solution concentrations of SMT and 3mSA for different solid phases at equilibrium with acetonitrile and methanol

Solvent	Solid phase at equilibrium	Invariant points (mole fraction) SMT	3mSA	Solvent	K_{sp} (M^2)
Acetonitrile	SMT + co-crystal	0.0041	0.0055	0.9903	8.0×10^{-3}
	3mSA + co-crystal	0.0013	0.0211	0.9775	1.1×10^{-2}
	Co-crystal	0.0016	0.0122	0.9861	7.6×10^{-3}
Methanol	SMT + co-crystal	0.0027	0.0125	0.9848	2.1×10^{-2}
	3mSA + co-crystal	0.0025	0.0144	0.9730	2.3×10^{-2}

point on the SMT–3mSA axis. Since in both solvents the stoichiometric line crosses through regions '2' and '3', formation of either solid SMT or a mixture of SMT and co-crystal is to be expected, depending on the evaporation end point.

Since in both solvents the co-crystal dissolves incongruently, co-crystal solubility determination *via* traditional techniques such as gravimetry is not possible as it relies on establishment of thermodynamic equilibrium between the solution and the co-crystal. However, in both solvents, we observe from Fig. 9, that the SMT solution concentration at the invariant point with solid SMT and co-crystal is higher than the SMT concentration in a binary system of solvent and solid SMT. Accordingly, dissolution of the pure 1 : 1 co-crystal in either solvent will lead to a solution having a higher SMT concentration than that obtained by dissolving pure solid SMT. Accordingly, from a pharmaceutical preformulation point of view, the co-crystal will potentially lead to a higher dissolution rate and thus potentially a higher bioavailability.

From a co-crystal manufacturing point of view, the pure SMT–3mSA co-crystal, in spite of the incongruency, can still be obtained by slurry conversion crystallization from a physical mixture of the two solid components in the solvent, if the overall composition is in the co-crystal region (region 6) of the phase diagram (Fig. 7 and 8). This requires an initial excess addition of the more soluble 3mSA than SMT, to place the conditions on the solubility curve of the co-crystal, then followed by addition of a suitable stoichiometric amount of each of the two pure solid components. The co-crystal formation can be initiated by addition of a smaller amount of co-crystal seeds.

In solution, a 1 : 1 co-crystal (AB) dissolves into API (A) and coformer (B) (eqn (3)) and the co-crystal solubility product (K_{sp}) is the product of activities of the API and the coformer in the solution at equilibrium (eqn (4)). If the activity coefficients are neglected, K_{sp} simplifies to the product of concentrations of A and B. This is analogous to ionic compounds, for which the constant K_{sp} refers to the product of ionic concentrations in the saturated solution and is proportional to the solubility.[37,38] The K_{sp} values in methanol and acetonitrile are given in Table 4 as calculated from the data of the invariant points. Notably, it is higher in methanol than in acetonitrile, signifying a higher co-crystal solubility in methanol. The difference in the K_{sp} values calculated from concentrations at the two invariant points, respectively, in the same solvent stems from the neglect of solution activity coefficients. If activity coefficients are accounted for, the K_{sp} should be equal in the two invariant points and in fact be independent of the solvent. Using eqn (5), and from the average K_{sp}, the values obtained for the co-crystal intrinsic solubility in acetonitrile and methanol are 0.094 mol L^{-1} and 0.148 mol L^{-1}, respectively.

$$AB \leftrightarrow A_{liq} + B_{liq} \tag{3}$$

$$K_{sp} = a_{A,liq}a_{B,liq} = \gamma_A[A]\gamma_B[B] \approx [A][B] \tag{4}$$

$$S_{AB} = \sqrt{K_{sp}} \tag{5}$$

$$\Delta G = -RT \ln\left(\frac{a_{liq}^{A+}a_{liq}^{B+}}{K_{sp}}\right) \tag{6}$$

Eqn (6) can be used to estimate the Gibbs energy of co-crystal formation from its pure, solid components, wherein a_{liq}^{A+} and a_{liq}^{B+} correspond to the activity of each solute in a solution in equilibrium with the pure solid components.[14,39] In approximating activities with concentrations the influence of concentration as well as the influence of the third component

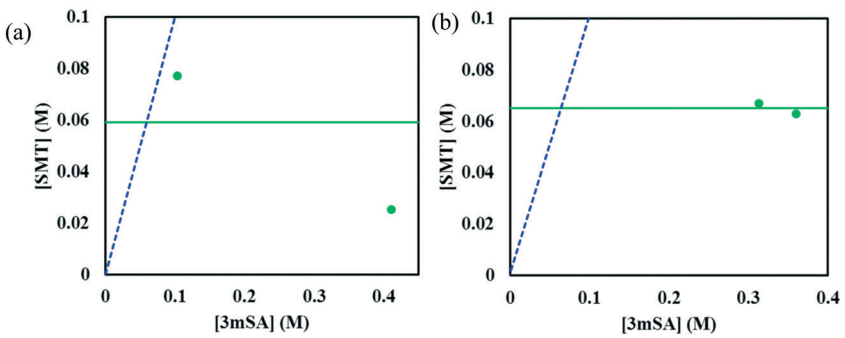

Fig. 9 Phase diagram of SMT–3mSA system in acetonitrile (a), and methanol (b). The horizontal green line corresponds to the solubility of pure SMT at 30 °C in each solvent. The points (filled circles) depict the invariant points at the same temperature. The blue dotted line is the 1 : 1 stoichiometric line.

on the activity coefficient of each component is neglected. As this influence is unknown, its neglect leads to uncertainty in the estimated Gibbs energy values. Using the average K_{sp} (see Table 4), the Gibbs energies of co-crystal formation estimates to become −2.3 kJ mol^{-1} (methanol data) and −5.0 kJ mol^{-1} (acetonitrile data), respectively. The negative values reveal that co-crystal formation from its pure solid components is a thermodynamically favoured process at 303 K. At higher temperature (406 K), the spontaneity of co-crystal formation has indeed been confirmed by DSC (Fig. 6).

As is shown in Table 5, the solubility ratio of the pure co-crystal components, *i.e.* coformer to API solubility, cannot be used to predict whether the co-crystal will dissolve congruently or incongruently. The data for the solubility ratio and dissolution behaviour of the SMT–salicylic system has been taken from previous work.[14]

With the change in solvent, the size of the region where co-crystal is the most stable solid phase changes appreciably. The size of this region can be estimated in terms of the area of a triangle, given by Heron's formula (eqn (7)). In Fig. 10b, the three vertices of the triangle in the ternary phase diagram are the stoichiometric point (R) and the two invariant points (P and Q); the coordinates represented as x, y, and z. Using the 3D-distance equation (eqn (8)), the lengths (d) of the edges 'PQ', 'QR', and 'PR' denoted as 'd_a', 'd_b', and 'd_c' respectively can be determined, which in turn can be used to determine the area 'A' represented by the purple region in Fig. 10b. Notably, the curvature of the co-crystal solubility line between the two invariant points, is neglected. Solubility ratio, denoted as 'r' refers to the coformer to API solubility ratio. The linear best fit between log (A) and log (r) is shown in the schematic in Fig. 10a. The regression coefficient, 0.94 depicts the linearity of the data. In Fig. 10a, data from an additional system, SMT–salicylic acid in methanol, acetonitrile and DMSO–methanol is included.[14] The three coordinates required for the calculation of the area (invariant points and co-crystal stoichiometric point) were extracted. An inverse relationship between 'r' and 'A', meaning a high coformer to API solubility ratio leads to a small co-crystal region and a low solubility ratio leads to a big co-crystal region in the ternary phase diagram.

$$s = \frac{d_a + d_b + d_c}{2}, A = \sqrt{s(s-d_a)(s-d_b)(s-d_c)} \quad (7)$$

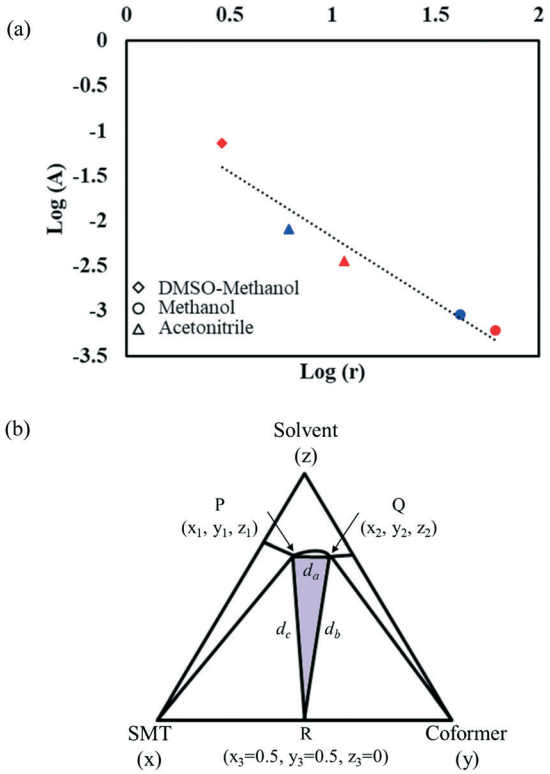

Fig. 10 Plot of log A (area of region in ternary phase diagram where co-crystal is the stable solid phase) *vs.* log r (ratio of coformer to API solubility). Red symbols correspond to the SMT–salicylic acid co-crystal;[14] blue symbols correspond to the SMT–3mSA co-crystal; different shapes represent different solvents (a); schematic representing the three vertices of the triangle *P, Q, R;* purple coloured region represents the area of the triangle (b).

$$d_{a,b,c} = \sqrt{(x_i - x_j)^2 + (y_i - y_j)^2 + (z_i - z_j)^2}; (i, j = 1, 2, 3, i \neq j) \quad (8)$$

Conclusions

A new 1 : 1 co-crystal between sulfamethazine and 3-methylsalicylic acid has been synthesized. The crystal structure has been solved and the co-crystal characterized by several techniques. The ternary phase diagram has been constructed in methanol and acetonitrile. The co-crystal exhibits incongruent dissolution in both solvents. Co-crystal formation from its solid components is shown to be

Table 5 The dissolution behaviour of two sulfamethazine co-crystals in different solvents

Co-crystal	Stoichiometry	Solvent	Solubility ratio (r)	Dissolution behaviour
Sulfamethazine–3-methylsalicylic acid	1 : 1	Acetonitrile	6.2	Incongruent
		Methanol	41.7	Incongruent
Sulfamethazine–salicylic acid[a]	1 : 1	Acetonitrile	11.5	Congruent
		Methanol	61.8	Incongruent
		DMSO–methanol	2.9	Incongruent

[a] Data taken from ref. 14.

spontaneous, with a negative Gibbs energy change, and endothermic, and hence driven by entropy increase. It is accompanied by an increase in molecular volume of at least 5%. The melting point of the co-crystal is 453.0 K, which is between the melting points of the pure API and coformer. The enthalpy of melting of the co-crystal is 56.6 kJ mol^{-1}, higher than that of both the API and coformer. The size of the region where co-crystal is stable, is inversely proportional to the solubility ratio of the coformer to API.

Conflicts of interest

There are no conflicts to declare.

Acknowledgements

This publication has emanated from research conducted with the financial support of the Swedish Research Council (Grant Number 2019-5059), the SSPC, the SFI Centre for Pharmaceuticals funded by Science Foundation Ireland (SFI), co-funded under the European Regional Development Fund under Grant Number 12/RC/2275, as well as support from the Bernal Institute and the Department of Chemical Sciences, both at the University of Limerick. The authors would like to acknowledge Peraka Krishna Sumanth for collecting single crystal XRD data.

References

1 R. Savla, J. Browne, V. Plassat, K. M. Wasan and E. K. Wasan, *Drug Dev. Ind. Pharm.*, 2017, **43**, 1743–1758.
2 B. M. Couillaud, P. Espeau, N. Mignet and Y. Corvis, *ChemMedChem*, 2019, **14**, 8–23.
3 N. K. Duggirala, M. L. Perry, Ö. Almarsson and M. J. Zaworotko, *Chem. Commun.*, 2016, **52**, 640–655.
4 C. B. Aakeröy, S. Forbes and J. Desper, *J. Am. Chem. Soc.*, 2009, **131**, 17048–17049.
5 S. F. Chow, M. Chen, L. Shi, A. H. Chow and C. C. Sun, *Pharm. Res.*, 2012, **29**, 1854–1865.
6 A. V. Trask, W. D. S. Motherwell and W. Jones, *Int. J. Pharm.*, 2006, **320**, 114–123.
7 Y. Corvis, P. Négrier, M. Lazerges, S. Massip, J.-M. Léger and P. Espeau, *J. Phys. Chem. B*, 2010, **114**, 5420–5426.
8 A. J. Smith, P. Kavuru, L. Wojtas, M. J. Zaworotko and R. D. Shytle, *Mol. Pharmaceutics*, 2011, **8**, 1867–1876.
9 S. Aitipamula, R. Banerjee, A. K. Bansal, K. Biradha, M. L. Cheney, A. R. Choudhury, G. R. Desiraju, A. G. Dikundwar, R. Dubey, N. Duggirala, P. P. Ghogale, S. Ghosh, P. K. Goswami, N. R. Goud, R. K. R. Jetti, P. Karpinski, P. Kaushik, D. Kumar, V. Kumar, B. Moulton, A. Mukherjee, G. Mukherjee, A. S. Myerson, V. Puri, A. Ramanan, T. Rajamannar, C. M. Reddy, N. Rodriguez-Hornedo, R. D. Rogers, T. N. G. Row, P. Sanphui, N. Shan, G. Shete, A. Singh, C. C. Sun, J. A. Swift, R. Thaimattam, T. S. Thakur, R. Kumar Thaper, S. P. Thomas, S. Tothadi, V. R. Vangala, P. Vishweshwar, D. R. Weyna and M. J. Zaworotko, *Cryst. Growth Des.*, 2012, **12**, 4290–4291.
10 S. L. Childs, G. P. Stahly and A. Park, *Mol. Pharmaceutics*, 2007, **4**, 323–338.
11 S. Kumar, *Indian J. Pharm. Sci.*, 2018, **79**, 858–871.
12 C. R. Groom, I. J. Bruno, M. P. Lightfoot and S. C. Ward, *Acta Crystallogr., Sect. B: Struct. Sci., Cryst. Eng. Mater.*, 2016, **72**, 171–179.
13 D. Ahuja, P. Bannigan and A. C. Rasmuson, *CrystEngComm*, 2017, **19**, 6481–6488.
14 D. Ahuja, M. Svärd and Å. C. Rasmuson, *CrystEngComm*, 2019, **21**, 2863–2874.
15 M. B. Hickey, M. L. Peterson, L. A. Scoppettuolo, S. L. Morrisette, A. Vetter, H. Guzmán, J. F. Remenar, Z. Zhang, M. D. Tawa and S. Haley, *Eur. J. Pharm. Biopharm.*, 2007, **67**, 112–119.
16 M. S. Jung, J. S. Kim, M. S. Kim, A. Alhalaweh, W. Cho, S. J. Hwang and S. P. Velaga, *J. Pharm. Pharmacol.*, 2010, **62**, 1560–1568.
17 D. P. McNamara, S. L. Childs, J. Giordano, A. Iarriccio, J. Cassidy, M. S. Shet, R. Mannion, E. O'Donnell and A. Park, *Pharm. Res.*, 2006, **23**, 1888–1897.
18 S. J. Nehm, B. Rodríguez-Spong and N. Rodríguez-Hornedo, *Cryst. Growth Des.*, 2006, **6**, 592–600.
19 G. L. Perlovich, *CrystEngComm*, 2017, **19**, 2870–2883.
20 www.prosim.net.
21 A. K. Basak, S. K. Mazumdar and S. Chaudhuri, *Acta Crystallogr., Sect. C: Cryst. Struct. Commun.*, 1983, **39**, 492–494.
22 M. P. Gupta and S. M. Prasad, *Acta Crystallogr., Sect. B: Struct. Crystallogr. Cryst. Chem.*, 1971, **27**, 713–717.
23 U. Patel, M. Haridas and T. Singh, *Acta Crystallogr., Sect. C: Cryst. Struct. Commun.*, 1988, **44**, 1264–1267.
24 P. C. Vioglio, M. R. Chierotti and R. Gobetto, *Adv. Drug Delivery Rev.*, 2017, **117**, 86–110.
25 J. Tolls, *Environ. Sci. Technol.*, 2001, **35**, 3397–3406.
26 J. Buckingham, *Dictionary of organic compounds*, CRC Press, 1996.
27 A. J. Cruz-Cabeza, *CrystEngComm*, 2012, **14**, 6362–6365.
28 M. Svärd, D. Ahuja and Å. C. Rasmuson, *Cryst. Growth Des.*, 2020, Manuscript under revision.
29 G. L. Perlovich, *CrystEngComm*, 2018, **20**, 3634–3637.
30 M. A. Oliveira, M. L. Peterson and R. J. Davey, *Cryst. Growth Des.*, 2011, **11**, 449–457.
31 A. O. Surov, K. A. Solanko, A. D. Bond, A. Bauer-Brandl and G. L. Perlovich, *CrystEngComm*, 2016, **18**, 4818–4829.
32 H. S. Chan, J. Kendrick, M. A. Neumann and F. J. Leusen, *CrystEngComm*, 2013, **15**, 3799–3807.
33 S.-W. Zhang, A. P. J. Brunskill, E. Schwartz and S. Sun, *Cryst. Growth Des.*, 2017, **17**, 2836–2843.
34 S.-W. Zhang, A. P. Brunskill, E. Schwartz and S. Sun, *Cryst. Growth Des.*, 2017, **17**, 2836–2843.
35 R. K. Tiwari, M. Haridas and T. P. Singh, *Acta Crystallogr., Sect. C: Cryst. Struct. Commun.*, 1984, **40**, 655–657.
36 G. R. Desiraju, *Cryst. Growth Des.*, 2011, **11**, 896–898.
37 S. N. Bhattachar, L. A. Deschenes and J. A. Wesley, *Drug Discovery Today*, 2006, **11**, 1012–1018.

38 D. J. Good and N. Rodríguez-Hornedo, *Cryst. Growth Des.*, 2009, **9**, 2252–2264.

39 S. Zhang and Å. C. Rasmuson, *CrystEngComm*, 2012, **14**, 4644–4655.